Mechanisms involved in the lipid membrane tubulation activity of the pH-responsive MakA protein from *Vibrio cholerae*

Athar Alam[1], Abdelbasset Yabrag[2,3], Naeem Ullah[2,3], Rasmus Sten[2,3], Jörgen Åden[2], Nandita Bodra[3,4], Hudson Pace[1,3,5], Marta Bally[1,3,5], Karina Persson[3,4], Bernt Eric Uhlin[2,3], Sun Nyunt Wai[2,3,6], Aftab Nadeem[2,3]

[1]Department of Clinical Microbiology, Umeå University, Umeå, Sweden

[2]Department of Molecular Biology, Umeå University, Umeå, Sweden

[3]Umeå Centre for Microbial Research (UCMR), Umeå University, Umeå, Sweden

[4]Department of Chemistry, Umeå University, Umeå, Sweden.

[5]Wallenberg Centre for Molecular Medicine, Umeå University, Umeå, Sweden

[6]The Laboratory for Molecular Infection Medicine Sweden (MIMS), Umeå University, Umeå, Sweden

Corresponding author: aftab.nadeem@umu.se

Abstract

Bacterial pore-forming toxins (PFTs) are key virulence factors that disrupt host cell membranes. The *Vibrio cholerae* cytotoxin MakA, a member of the ClyA structural family of α-PFTs, exhibits a unique, pH-dependent ability to induce lipid membrane tubulation. This study elucidates the molecular mechanisms underlying this process. We identify the N-terminal histidine residue (His30) of MakA as a critical pH sensor that is indispensable for membrane tubulation but not required for membrane binding and cell lysis. Substitution of His30 with lysine, $MakA^{H30K}$, abrogated tubulation without affecting membrane insertion, instead triggering aberrant membrane fusion events. Circular dichroism spectroscopy analysis revealed that the $MakA^{H30K}$ substitution attenuates the robust α-helical transition observed in wild-type MakA upon lipid membrane binding, providing a molecular explanation for its functional defect. Furthermore, we established that membrane cholesterol contributes to MakA-induced tubulation of lipid membranes, as its absence or mutation of a putative cholesterol-binding motif $MakA^{I236D\&I237D}$ abolishes both membrane association and tubule formation. A key implication of our work is the mechanistic uncoupling of membrane tubulation from cytolysis, revealing that MakA can perturb membranes via distinct pathways. These findings define a sophisticated activation mechanism where His30 protonation in the acidic host environment and specific cholesterol binding synergistically drive the conformational change necessary for helical oligomerization and membrane tubulation. We discuss our findings from the viewpoint of possible convergent evolution, where bacterial PFTs like MakA partly may mimic ancient membrane remodelers involved in membrane repair pathways, such as ESCRT-III, but for bacterial fitness in host interactions and pathogenesis. Moreover, the present study provides a foundation for possible development of therapeutic strategies aimed at inhibiting these critical interactions.

Introduction

Bacteria have evolved a remarkable array of strategies to interact with host organisms, and among the most effective virulence factors are proteins that directly compromise cellular membranes. A broad class of these effectors is represented by pore-forming toxins (PFTs), which are secreted as soluble proteins that can undergo conformational rearrangements upon binding to host membranes, eventually inserting into lipid bilayers to generate pores. This process not only disrupts membrane integrity but also triggers a cascade of cellular responses that range from ion imbalance and signaling alterations to cell death [1-4]. PFTs are found across a wide spectrum of bacterial pathogens, both Gram-positive and Gram-negative, and play critical roles in colonization, nutrient acquisition, immune evasion, and microbial competition. Structurally, they are classified into two broad families: α-PFTs, which employ α-helical structures for membrane penetration, and β-PFTs, which form β-barrel pores [3]. Despite structural diversity, the unifying hallmark of PFTs is their capacity to oligomerize on membranes and create aqueous channels that compromise selective permeability.

Vibrio cholerae, the etiological agent of cholera, is a paradigmatic example of Gram-negative bacterium that uses an array of toxins to establish infection. The classical virulence determinants are cholera toxin (CT) and the toxin co-regulated pilus (TCP), both of which are essential for the severe diarrheal disease associated with epidemic strains [5]. However, environmental isolates that lack CT and TCP remain pathogenic and have been implicated in secretory diarrhea, wound infections, and septicemia [6, 7]. These strains frequently carry alternative virulence factors, including hemolysins, proteases, RTX toxins, and lipases [7]. Among these, a newly characterized cytotoxin, motility-associated killing factor A (MakA), has emerged as an important fitness factor for *V. cholerae* in its interactions with predators in natural environments and was identified through studies with *Caenorhabditis elegans* and zebrafish infection models [8]. The *makA* gene (vca0883) resides within a five-gene cluster (*makDCBAE*) that is widely conserved among *V. cholerae* isolates [8-10]. Structural studies demonstrated that MakA belongs to the ClyA family of α-PFTs, named after the *Escherichia coli* cytotoxin ClyA [8, 11, 12].

The Mak proteins represent a distinctive subfamily of PFTs. Biochemical analyses revealed that MakA can combine with MakB and MakE to form a tripartite cytolytic complex, while none of these components alone can induce pore formation [9]. This organization resembles other multicomponent α-PFTs, such as YaxAB from *Yersinia enterocolitica* [13], XaxAB from *Xenorhabdus nematophila* [14], and tripartite toxins such as NheABC and HblL1L2B from *Bacillus cereus* [15], AhlABC from *Aeromonas hydrophila* [16], and SmhABC from *Serratia marcescens* [17]. In each case, pore formation depends on the concerted action of all components, often following a precise assembly sequence to maximize cytolytic efficiency [9, 16, 17]. In the case of *V. cholerae*, an equimolar mixture of MakA, MakB, and MakE can assemble into pores in mammalian membranes, underscoring the physiological relevance of this complex [9]. The secretion of MakA, MakB and MakE proteins from *V. cholerae* occurs primarily in a flagellum-dependent manner [8, 9]. Remarkably, *in vitro* studies revealed that MakA alone exerts several

independent cellular effects including autophagy modulation, G2/M cell cycle arrest, and apoptosis in cultured epithelial cells [18-20]. Importantly, our recent structural study revealed that MakA possesses a unique, pH-dependent activity distinct from canonical pore formation [21]. Upon exposure to acidic conditions (pH ≤6.5), mimicking the endolysosomal compartment, soluble MakA monomers undergo a large conformational change. The N-terminal head and neck domains refold into transmembrane helices, a process triggered by the protonation of key residues and the unfolding of a protective C-terminal β-tongue. This 'activated' form inserts into lipid membranes and oligomerizes into unique helical filaments that internalize a thin annular lipid bilayer, rather than forming a classic pore. The oligomerization of MakA drives the formation of high-curvature tubular protrusions that deplete membrane integrity, leading to cytolysis and hemolysis [21]. This pH-dependent mechanism ensures that the MakA activation is precisely targeted within the acidic host environment.

Environmental pH gradients are critical regulators of bacterial virulence, modulating the activity of many membrane-associated proteins. One prominent example is the Phage Shock Protein A (PspA), a bacterial homolog of the Endosomal Sorting Complex Required for Transport-III (ESCRT-III) superfamily. Structural analyses of Synechocystis PspA have shown that its conformational flexibility and ability to assemble into diverse tubular structures underline its pH- and nucleotide-dependent membrane-remodeling activity [22,23]. Notably, PspA possesses intrinsic ATPase activity, and mutations in key residues (R44, E126, and E179) abolish both ATP hydrolysis and membrane remodeling, establishing a direct mechanistic link between nucleotide turnover and function. These findings identify PspA and its homologs as founding members of an ancient ESCRT-III-like superfamily in bacteria, capable of sensing and repairing membrane damage.

The pH-sensing and membrane-remodeling properties of MakA represent a novel extension of this paradigm. Although MakA remains structurally stable across a broad pH range, its membrane tubulation activity is specifically triggered at mildly acidic conditions (pH 5–6.5), mimicking the intestinal environment of the predator model host organism *C. elegans* [21]. Understanding the molecular basis of this pH-dependent activation is therefore crucial to elucidating how *V. cholerae* fine-tunes its virulence mechanisms and potentially exploits ESCRT-III-like strategies to remodel host membranes.

In this study, we investigate the hypothesis that the N-terminal domain of MakA is essential for its membrane perturbation activity under the mildly acidic pH. Building on the observation that this particular MakA activity is pH-dependent, and inspired by the mechanism of nucleotide-sensing in PspA [22, 23], we identified a histidine residue (His30) within the N-terminal domain as a putative pH sensor. We demonstrate that protonation of His30 at acidic pH triggers the conformational rearrangements required for membrane insertion and oligomerization. Substitution of His30 with lysine ($MakA^{H30K}$) abolishes this pH response, effectively eliminating the membrane tubulation activity while preserving membrane binding. These findings reveal that MakA contain a sophisticated pH-sensing mechanism, integrating environmental and lipid cues for its activation.

We propose that this mechanism reflects an evolutionarily conserved strategy, reminiscent of ESCRT-III–like membrane remodelers.

124 # Results
125
126 **The histidine residue at the N-terminus of the MakA facilitates tubulation of the target cell**
127 **membrane**
128 Under mildly acidic conditions, MakA binds to lipid membranes and induces pronounced
129 tubulation [21]. To investigate whether this process requires membrane insertion, we labeled
130 human erythrocytes with the lipophilic dye Dil and incubated them with either unlabeled MakA or
131 Alexa488-labeled MakA (Alexa488-MakA) for 4 hours at pH 6.5, followed by confocal
132 microscopy analysis (**Fig. 1A–B**). The results suggest that MakA inserts into the erythrocyte
133 membrane, as evidenced by the co-localization of Alexa488-MakA with the membrane (**Fig. 1B**).
134 Line profile analysis further validated this co-localization along the tubules (**Fig. 1B**).
135 Given the known role of histidine residues in pH sensitive molecular switch [24], we substituted
136 three histidine residues located in the N-terminal and head domains of MakA with lysine,
137 generating the MakA^{H30K}, MakA^{H95K}, and MakA^{H151K} mutant proteins (**Fig. 1C, and Fig. S1A-B**).
138 Based on our recently resolved cryo-EM structural model of membrane-bound MakA, which
139 suggests a homodimeric assembly [21], we also examined the contribution of the adjacent N-
140 terminal cysteine (Cys29) to membrane remodeling. To assess the impact of side-chain polarity
141 and hydrophobicity, Cys29 was substituted with either alanine (MakA^{C29A}) or serine (MakA^{C29S})
142 (**Fig. 1C, and Fig. S1A-B**).
143 All MakA mutants were successfully expressed and purified in soluble form, except MakA^{H151K,}
144 which exhibited poor solubility and was therefore excluded from further analysis. The purity of
145 wild-type and mutant MakA proteins was assessed via SDS-PAGE analysis (**Fig. S1B**). To evaluate
146 membrane remodeling activity, Dil-labeled erythrocytes were incubated with each MakA protein
147 (1 μM, 4 hours at pH 6.5) and analyzed by confocal microscopy (**Fig. 1D**). Both MakA^{H95K} and
148 MakA^{C29S} retained the ability to induce membrane tubulation comparable to wild-type MakA. In
149 contrast, MakA^{H30K} and MakA^{C29A} failed to induce tubulation (**Fig. 1D, and Fig. S2**). Notably,
150 substitution of Cys29 with alanine (MakA^{C29A}) completely abolished MakA activity, whereas
151 replacement with serine (MakA^{C29S}) preserved function, highlighting the importance of side chain
152 polarity rather than thiol reactivity at this position. Intriguingly, MakA^{H30K} triggered aberrant
153 membrane fusion events, a phenotype not observed in case of wild-type MakA (**Fig. 1D, and Fig.**
154 **S2**). These findings were corroborated by scanning electron microscopy (SEM), which revealed
155 distinct tubular structures on erythrocyte surfaces treated with wild-type MakA and MakA^{H95K}, but
156 not with MakA^{H30K} (**Fig. 1E**). Overall, the data underscores the importance of specific N-terminal
157 residues, particularly His30 and Cys29 were critical for the structural transitions that enable MakA-
158 mediated membrane binding and tubulation.
159
160 **Histidine-30 is critical for the pH-sensitive conformational change required for MakA-**
161 **mediated tubulation**
162 To assess whether substitution of the N-terminal histidine residue affects membrane binding, we
163 incubated Dil-labeled erythrocytes with Alexa488-labeled wild-type MakA, MakA^{H30K}, or

164 MakA^{H95K} for 4 hours at pH 6.5 and analyzed the samples by confocal microscopy. Both MakA^{H30K}
165 and MakA^{H95K} mutant proteins were localized to the erythrocyte membrane similarly to wild-type
166 MakA, indicating that these mutations do not impair membrane association (**Fig. 2A**). Despite
167 similar membrane binding, the MakA^{H30K} variant failed to induce tubulation, underscoring that
168 while His30 is dispensable for membrane association, it is vital for pH-dependent conformational
169 activation that drives membrane remodeling. In contrast, the MakA^{H95K} retained tubulation activity
170 comparable to wild-type MakA (**Fig. 2A**).
171 To determine whether the loss of tubulation in MakA^{H30K} was specific to the complex erythrocyte
172 membrane environment or reflected a general defect in lipid remodeling, we extended our analysis
173 to reconstituted lipid bilayers. Liposomes prepared from epithelial cell lipid extracts (ECLE) were
174 incubated with wild-type MakA, MakA^{H30K}, or MakA^{H95K} (3 μM, 90 min at pH 6.5) and analyzed
175 by transmission electron microscopy (TEM). Consistent with the erythrocyte data, both native
176 MakA and the MakA^{H95K} induced robust liposome tubulation whereas MakA^{H30K} did not (**Fig. 2B**).
177 To ascertain whether this attenuated conformational response in the MakA^{H30K} mutant was due to
178 a loss of lipid binding, we exposed liposomes to native Alexa488-MakA, Alexa488-MakA^{H30K} or
179 Alexa488-MakA^{H95K} (1 μM, 90 min at pH 6.5) and examined them by confocal microscopy. All
180 proteins bound efficiently to liposomes (**Fig. 2C**), indicating that the loss of tubulation by
181 MakA^{H30K} was not due to a defect in membrane binding. Liposome co-sedimentation (pull-down)
182 assays further confirmed comparable lipid association across variants (**Fig. 2D**).
183 We next investigated the binding kinetics of MakA and histidine substitution mutants, i.e.,
184 MakA^{H30K} and MakA^{H95K}, to liposomes prepared from ECLE using SparkCyto imaging system
185 (**Fig. 2E-F**). Data analysis indicates that MakA and those mutants (MakA^{H30K} and MakA^{H95K}) have
186 similar binding profiles for liposomes prepared from ECLE. Importantly, there was no significant
187 difference in linear rate constant per hour among the mutant proteins and wild-type MakA (**Fig.
188 2E**). Collectively, these results demonstrate that His30 was not required for membrane binding but
189 appeared indispensable for the pH-sensitive conformational change that enables MakA-driven
190 membrane tubulation.
191
192 **Histidine-30 is dispensable for membrane lysis but critical for membrane fusion**
193 A hallmark of many membrane-active proteins, such as PFTs and antimicrobial peptides, is their
194 ability to undergo a conformational transition from a disordered state in solution to an α-helical
195 structure upon membrane association [25, 26]. To investigate whether the MakA^{H30K} or MakA^{H95K}
196 substitution mutations would have an impact on conformational change compared to the wild-type
197 MakA, we analyzed their secondary structures at pH 6.5 using circular dichroism (CD)
198 spectroscopy in the presence and absence of liposomes. The far-UV CD spectra of all three proteins
199 in solution were nearly identical, indicating that the substitution mutations do not cause major
200 structural alterations under these conditions (**Fig. 3A**). Upon the addition of liposomes, all proteins
201 exhibited the characteristic increase in α-helical content, evidenced by a significant intensification
202 of the minima at 208 nm and 222 nm (**Fig. 3B**). Quantitative comparison of the spectral changes
203 (**Table S1**) revealed that the MakA^{H95K} mutant protein underwent conformational reorganization

204 comparable to the wild-type MakA. In contrast, the MakA^{H30K} mutant displayed a markedly
205 attenuated helical transition, suggesting it fails to adopt the fully active, membrane-bound
206 conformation required for efficient tubule formation. This structural defect provides a plausible
207 molecular explanation for its inability to induce membrane tubulation.
208 We have previously demonstrated that MakA induces hemolysis of erythrocytes when tested at
209 acidic pH [21]. However, a potential mechanistic link between MakA-induced membrane
210 tubulation and cell lysis has remained unclear. To investigate whether membrane tubulation is a
211 prerequisite for MakA-mediated lysis, we examined the hemolytic activity of wild-type MakA and
212 the histidine substitution mutant proteins (MakA^{H30K} and MakA^{H95K}) using both confocal
213 microscopy and quantitative hemolysis assays (**Fig. 3C-D**). Confocal microscopy of Dil-labeled
214 erythrocytes exposed to MakA proteins for 4 hours at pH 6.5 revealed comparable levels of
215 membrane disruption across all conditions (**Fig. 3C**). Notably, despite its inability to induce
216 membrane tubulation, the MakA^{H30K} variant still caused erythrocyte lysis, indicating that tubulation
217 is an essential prerequisite for membrane rupture. This observation was supported by quantitative
218 hemolysis assays, which showed similar levels of hemoglobin release from the erythrocytes treated
219 with native MakA and its histidine mutants, MakA^{H95K} and MakA^{H30K} respectively (**Fig. 3D).**
220 Interestingly, while MakA^{H30K} failed to induce tubulation (**Fig. 1D and Fig. 2A-B**), it promoted
221 membrane fusion events between erythrocytes, a phenotype not observed in cells treated with
222 native MakA and MakA^{H95K}. These fusion events, however, did not correlate with increased
223 hemolysis, suggesting that fusion and lysis represent mechanistically distinct outcomes of MakA-
224 membrane interactions. Together, these results demonstrate that while His30 is not required for
225 MakA-mediated membrane lysis, it plays a critical role in promoting the conformational and
226 structural rearrangements necessary for membrane fusion and tubulation.
227
228 **Cholesterol is promoting MakA-induced membrane tubulation**
229 Cellular membranes are composed of diverse lipid species, among which cholesterol is a key
230 structural component in modulating membrane properties of erythrocytes and other mammalian
231 cells [27]. Our previous work demonstrated that MakA binds to synthetic lipid membranes (SLMs)
232 of defined composition, including cholesterol, and induces pronounced membrane tubulation [21].
233 Notably, we also observed tubulation induced by MakA at acidic pH on liposomes prepared with
234 lipids extracted from *C. elegans* or *E. coli*, organisms that lack cholesterol [21]. To further delineate
235 the specific lipid requirements underlying this process, we systematically tested MakA activity on
236 SLM variants differing in lipid composition. TEM analysis of SLM liposomes exposed to MakA
237 (3 μM, 90 min at pH 6.5) revealed robust tubulation occurred in all tested SLM variants except
238 those lacking cholesterol (**Fig. 4A**). This finding indicates that cholesterol can be a critical
239 component required for MakA-induced membrane remodeling in mammalian cells. To determine
240 whether cholesterol is required for MakA membrane association, we incubated SLM liposomes
241 containing or lacking cholesterol with Alexa568-MakA (3 μM, 4 hours at pH 6.5) and analyzed
242 binding by confocal microscopy. The results showed a marked reduction in MakA binding and

243 liposome aggregation in the absence of cholesterol (**Fig. 4B**), suggesting that cholesterol facilitates
244 MakA attachment and subsequent structural reorganization of the membrane.
245 To further dissect the molecular basis of this cholesterol dependence, we examined the
246 MakA$^{I236D\&I237D}$ mutant protein in which the hydrophobic residues Ile236 and Ile237 were
247 substituted with aspartic acid (**Fig. S1A**). Those residues were previously implicated in cholesterol
248 recognition by MakA [28]. Circular dichroism (CD) spectroscopy revealed minimal changes in
249 secondary structure among MakA and the MakA$^{I236D\&I237D}$ mutant (**Fig. 4C**) indicating that the
250 overall protein fold remained intact. Functionally, however, the MakA$^{I236D\&I237D}$ mutant protein
251 failed to induce tubulation in both erythrocyte membranes and SLM liposomes, in contrast to wild-
252 type MakA (**Fig. 4D-E**). Collectively, these results demonstrate that cholesterol strongly promoted
253 MakA-mediated membrane tubulation on the tested SLM liposomes. The requirement for
254 cholesterol likely reflects its dual role in promoting MakA binding and facilitating the
255 conformational rearrangements necessary for membrane deformation.
256

Discussion

The MakA protein is the first α-PFT protein family member from *V. cholerae* shown to possess the ability to induce lipid membrane tubulation [21]. In this study, we aimed to identify key molecular determinants underlying the membrane-active properties of *V. cholerae* MakA. The N-terminus (2-42 residues) of MakA has been previously implicated in membrane interaction [18]; however, the specific amino acid residues mediating this interaction remained undefined. Our present study revealed that the N-terminal histidine residue (His30) is indispensable for acid sensing and membrane tubulation and that cholesterol serves as a cofactor required for MakA-induced membrane remodeling of synthetic lipid membranes. Furthermore, we found that His30 was not required for hemolysis activity, suggesting that membrane tubulation and lysis at pH 6.5 arise from distinct mechanistic pathways. Substitution of His30 with lysine ($MakA^{H30K}$) abrogated tubulation without affecting membrane binding, as evidenced by multiple complementary approaches, including confocal microscopy, transmission- and scanning- electron microscopy, and liposome co-sedimentation assays. Histidine residues are well known as molecular pH sensors due to the proximity of their side-chain pKa to physiological pH, allowing them to undergo reversible protonation and deprotonation in response to environmental acidification [24]. The importance of histidine-mediated conformational rearrangements in membrane-active toxins has been demonstrated for several bacterial PFTs, where protonation drives structural transitions required for membrane insertion and oligomerization [29-32]. Our results extend this paradigm to MakA by demonstrating that His30 is specifically required for the transition from a membrane-bound to a tubulation-competent conformation. The $MakA^{H30K}$ mutant protein, while capable of binding and partially inserting into membranes, fails to undergo the robust α-helical transition observed in wild-type MakA upon lipid interaction, as shown by CD spectroscopy. This attenuated conformational response likely underlies its inability to induce membrane tubulation. Interestingly, the $MakA^{H95K}$ mutant protein, in which a histidine residue close to the head domain is substituted, retained both membrane binding and tubulation activity, indicating that the N-terminal His-30 plays a unique and non-redundant role in acid sensing and structural activation. This specificity is further supported by our observation that the $MakA^{H30K}$ mutant protein, but not $MakA^{H95K}$, induces membrane fusion events, suggesting that His30 may also influence the mode of membrane remodeling. The ability of MakA to induce different membrane perturbances depending on its structural state and the lipid environment underscores the versatility of this protein to affect cell membranes via diverse molecular mechanisms.

Mammalian cellular membranes are composed of diverse lipid species, with cholesterol serving as a key structural determinant of membrane rigidity, curvature, and microdomain organization [27]. Our data demonstrate that MakA activity is strongly promoted by cholesterol for effective membrane binding and tubulation. Absence of cholesterol abrogated MakA association with synthetic lipid membranes and markedly reduced liposome aggregation, indicating that cholesterol directly facilitates MakA–membrane interactions. Furthermore, substitution of two hydrophobic residues (Ile236 and Ile237), previously implicated in cholesterol recognition, with negatively

charged aspartic acids MakA$^{I236D\&I237D}$ variant [28] abolished MakA's ability to bind membranes and induce tubulation. This finding supports the notion that MakA recognizes and exploits cholesterol-rich domains, such as lipid rafts, as platforms for membrane remodeling. Similar cholesterol-promoted membrane sculpting has been reported for eukaryotic proteins such as caveolin-1 (Cav-1), which binds to cholesterol-rich domains to generate positive curvature and induce tubulation [4]. Thus, MakA may mimic or exploit host-like mechanisms of membrane remodeling to perturb cellular integrity during predator/host interactions.

Our findings demonstrate that MakA can induce tubulation in lipid membranes of liposomes derived from diverse biological sources, including human epithelial cell extracts, *E. coli* total lipid extracts, and *C. elegans* total lipid extracts. This broad activity suggests that MakA recognizes conserved physicochemical membrane features rather than some specific lipid composition(s). In liposomes prepared from a synthetic lipid mixture (SLM), however, membrane tubulation was strictly dependent on the presence of cholesterol, highlighting a critical role for sterols in facilitating MakA-mediated membrane remodeling. This sterol dependence is consistent with evidence that cholesterol-driven changes in membrane order, rigidity, and organization facilitate pore-forming toxin (PFT) binding, insertion, and oligomeric assembly [33]. The *E. coli* lipid extracts are primarily composed of phosphatidyl ethanolamine (PE), phosphatidylglycerol (PG), and cardiolipin (CL), with PE as the most abundant neutral lipid and anionic PG and CL conferring a net negative charge [34, 35]. The *E. coli* total lipid extract may support tubulation through mechanisms independent of sterols. Notably, CL accumulates in highly curved membrane regions, and its conical shape favors curvature, presumably lowering the energetic barrier for MakA-induced tubule formation and potentially enabling direct interactions that promote membrane remodeling [36, 37]. In contrast, *C. elegans* membranes, dominated by PC and PE glycerophospholipids, may contain very low levels of cholesterol [38-40]. The observation that MakA can still induce tubulation in these membranes suggests that even trace amounts of sterols may suffice for MakA activity. Such low-level sterols may derive from dietary uptake under laboratory conditions, where *C. elegans* relies entirely on exogenous sources for sterol acquisition [41]. This highlights the intriguing possibility that MakA can exploit minimal sterol content to initiate membrane curvature, pointing to a high sterol sensitivity or a cooperative mechanism with other lipid species. MakA-induced tubulation in these membranes suggests that MakA may interact with a broader spectrum of sterols than previously recognized, although differences in sterol structure could influence efficiency or mechanistic details. These observations emphasize the need to dissect sterol-specific contributions to MakA activity and to understand whether MakA distinguishes between sterols in facilitating membrane insertion, oligomerization, or curvature induction. Together, these findings highlight MakA's versatility in remodeling membranes with diverse lipid compositions and point to key unanswered questions about sterol recognition and its implications for PFT function, membrane biophysics, and predator/host–pathogen interactions across evolutionary distances.

MakA-induced membrane remodeling resembles processes mediated by integral and peripheral membrane proteins that sculpt membranes through hydrophobic insertion or scaffolding

337 mechanisms. For instance, integral membrane proteins such as reticulons and A17, encoded by
338 poxvirus, generate high-membrane-curvature structures like vesicles and tubules through
339 hydrophobic domains with intrinsic shapes, such as conical or inverted conical transmembrane
340 domains [42, 43]. Reticulons, with their short hairpin transmembrane domains, occupy more space
341 in the outer leaflet, adopting an inverted cone shape that drives curvature, while A17 forms
342 crescent-shaped viral structures with tubules as small as 25 nm in diameter [42, 43]. Similarly,
343 FAM134B, an endoplasmic reticulum (ER)-resident protein, uses two wedge-shaped
344 transmembrane hairpin domains to generate high membrane curvature in the ER, facilitating
345 vesicle formation for phagosomal engulfment [44, 45]. Similar to MakA, peripherin-2/rds and the
346 influenza virus M2 protein induces tubulovesicular membrane foci by inserting its amphipathic α-
347 helices (AH) in cholesterol rich lipid membranes [46]. MakA appears to follow a comparable
348 strategy: upon acid-induced activation and cholesterol binding, its amphipathic α-helices
349 reorganize into oligomeric filaments that drive local curvature and membrane protrusion.
350 Moreover, MakA's membrane remodeling activity draws intriguing parallels with the eukaryotic
351 ESCRT-III complex, which plays a critical role in membrane repair and scission [47]. While MakA,
352 as a bacterial protein has presumably evolved to disrupt membranes in a pH-dependent manner to
353 promote *V. cholerae* fitness against predatory organisms, ESCRT-III functions to restore membrane
354 integrity to maintain cellular homeostasis, such as in multivesicular body (MVB) formation,
355 cytokinesis, and wound repair [22]. Despite their seemingly opposing roles, both systems rely on
356 dynamic α-helical assemblies capable of inducing extreme curvature. MakA induces high-
357 curvature tubulation (~25-50 nm diameter tubules) through pH-dependent oligomerization into
358 helical filaments, promoted by cholesterol binding and His30-mediated conformational changes.
359 ESCRT-III subunits (e.g., CHMP proteins) polymerize into spirals to constrict membranes during
360 intraluminal vesicle formation or wound repair. Although MakA lacks sequence homology to
361 ESCRT-III components, the structural resemblance of their helical assemblies suggests convergent
362 evolution, whereby MakA may exploit similar biophysical principles for destructive remodeling.
363 Notably, host cells have been shown to recruit ESCRT-III machinery to repair pores generated by
364 bacterial PFTs [23], raising the possibility that MakA-induced damage may trigger compensatory
365 ESCRT-dependent repair responses.
366 A striking observation from the current study is that the His30 residue, while essential for
367 tubulation, was not required for MakA-mediated hemolytic activity at acidic pH. The $MakA^{H30K}$
368 variant, despite its inability to induce tubulation, retains hemolytic activity, as demonstrated by
369 confocal microscopy and quantitative hemolysis assays. This observation demonstrated that
370 membrane tubulation and lysis are mechanistically distinct processes. Tubulation likely reflects a
371 specialized structural state of MakA optimized for membrane remodeling, whereas lysis results
372 from alternative, perhaps less ordered, modes of membrane disruption. This functional bifurcation
373 is reminiscent of cholesterol-dependent cytolysins (CDCs), which can exist in distinct pre-pore and
374 pore-forming states, or antimicrobial peptides that induce a spectrum of membrane perturbation,
375 from transient leakage to catastrophic rupture, depending on concentration and lipid composition

[48, 49]. Our data thus suggests that MakA possesses multiple membrane-active configurations that enable it to exert diverse biophysical effects on host membranes.

In summary, this study reveals that the His30 residue acts as a molecular pH sensor mediating MakA's conformational activation, while cholesterol serves as a structural cofactor that promotes membrane binding and tubulation. Together, these factors orchestrate MakA's ability to remodel, fuse, and rupture membranes through distinct but interrelated mechanisms. These findings provide fundamental insights into how this protein from *V. cholerae* can be employed for manipulation of mammalian cell membranes and establish a conceptual framework for exploring bacterial protein–membrane interactions for possible biotechnological applications.

386 # Material and Methods

387 **Purification of native MakA and its variants**

388 The cloning, expression, and purification strategy for native MakA has been described previously
389 [8]. To engineer the substitution mutants at the N-terminal of MakA (designated $MakA^{C29A}$,
390 $MakA^{C29S}$ $MakA^{H30K}$, $MakA^{H95K}$, and $MakA^{H151K}$) or the head domain of $MakA^{I236D\&I237D}$, the
391 wild-type MakA plasmid served as the template for site-directed mutagenesis using the
392 QuikChange XL-II kit (Stratagene). The desired substitution mutation was confirmed by DNA
393 sequencing. The primers used for this mutagenesis were: MakA_C29A-F 5'-tgt gtt taa aat ggc atg
394 ggc ctg cgc tgt gat gac tgt g-3', MakA_C29A-R 5'- cac agt cat cac agc gca ggc cca tgc cat ttt aaa
395 cac a-3'; MakA_C29S-F 5'-cag tca tca cag cgc aga gcc atg cca ttt taa ac-3', MakA_C29S-R 5'-gtt
396 taa aat ggc atg gct ctg cgc tgt gat gac tg-3',; MakA_H30K_R 5'-aat tgt gtg ttt aaa atg gcc ttg cac tgc
397 gct gtg atg act g-3', MakA_H30K_F 5'-cag tca tca cag cgc agt gca agg cca ttt taa aca cac aat t-3';
398 MakA_H95K_R 5'-gtt gga tcc gct tta tat aac tcc tta atg gca tcg att gat gct tga a-3', MakA_H95K_F
399 5'-ttc aag cat caa tcg atg cca tta agg agt tat ata aag cgg atc caa c-3'; MakA_H151K_R 5'-gca cca ttg
400 act aag tca tcc ttt gct gct tgc att ttc acc c-3', MakA_H151K_F 5'-ggg tga aaa tgc aag cag caa agg
401 atg act tag tca atg gtg c-3'. For protein expression, *E. coli* BL21(DE3) LysS cells (Novagen) were
402 transformed with plasmids encoding either the wild-type or mutant MakA proteins. Cultures were
403 grown to an OD_{600} of approximately 0.8, at which point protein expression was induced with 1 mM
404 IPTG. Following induction, cells were harvested by centrifugation at 4 °C. Protein purification was
405 carried out using Ni-NTA affinity chromatography. The N-terminal His_6-tag was cleaved using
406 TEV protease, and the mixture was passed through a second Ni-NTA column to remove uncleaved
407 protein and protease. The resulting protein was concentrated using Amicon Ultra-15 centrifugal
408 filters with a 10 kDa molecular weight cutoff (Millipore) and further purified by size-exclusion
409 chromatography on a HiLoad 16/60 Superdex 200 pg column (GE Healthcare) equilibrated in PBS
410 (pH 7.4). Protein purity was assessed by SDS-PAGE. Purification of $MakA^{H151K}$ was not performed
411 due to its inability to remain in soluble form.
412 Fluorescent labeling of both wild-type MakA and mutant proteins were performed using the Alexa
413 Fluor 488 or Alexa Fluor 568 Protein Labeling Kit (Thermo Fisher Scientific), following the
414 manufacturer's instruction.
415

416 **Circular dichroism spectroscopy**

417 Far-UV circular dichroism (CD) spectra of wild-type MakA and the mutant proteins ($MakA^{H30K}$,
418 $MakA^{H95K}$, $MakA^{I236D,I237D}$) were recorded, with or without ECLE liposome complexes, using a
419 Jasco J-720 spectropolarimeter (Jasco, Japan) at 25 °C. Protein samples (3 μM) and ECLE
420 liposomes (1 mg/mL) were incubated overnight at 25°C in either citrate (pH 6.5) or phosphate
421 buffer (pH 6.5). Measurements were conducted in a 0.1 cm path length quartz cuvette with a
422 bandwidth of 2 nm. Spectra were collected over the 190–260 nm range, averaged across five scans,
423 and corrected by subtracting the corresponding buffer baseline. All measurements were performed
424 under identical conditions to ensure comparability across variants. The reproducibility of spectra
425 was confirmed by repeated scans, and no significant baseline drift was observed.

426
427 **Human erythrocyte hemolysis assay**
428 Freshly prepared human erythrocytes (0.25%) suspended in citrate buffer (120 mM sodium citrate,
429 pH adjusted to 7.4, 6.5 and 5.0) were incubated with increasing concentrations of MakA or
430 $MakA^{H30K}$ or $MakA^{H95K}$ mutant proteins in Eppendorf tubes for 5 hours at 37°C. Following
431 incubation, samples were centrifuged at (500 × *g*) for 10 min, and the supernatants were collected.
432 Hemoglobin release, indicative of red blood cell lysis, was quantified spectrophotometrically by
433 measuring absorbance at 415 nm. Hemolysis induced by MakA or its mutants was normalized to
434 erythrocytes treated with 0.1% Triton X-100 (set as 100% lysis). Data are presented as the
435 percentage of total hemolysis relative to the Triton X-100 treated cells.
436
437 **Extraction of epithelial cell lipids for liposome binding assays**
438 Lipids were extracted by the Folch method (Folch et al., 1957) from 10 × 150 cm^2 confluent flasks
439 of HCT8 cells. Briefly, the lipid extracts dissolved in chloroform were dried to a thin film under a
440 gentle nitrogen stream, yielding approximately 12 mg of total lipid. The dried lipid film (5 or 10
441 mg/mL) was hydrated in one of the following buffers: HEPES buffer (10 mM HEPES, 150 mM
442 NaCl, pH 7.4), or citrate buffer (120 mM citrate buffer, pH 6.5). The resulting lipid suspensions
443 were extruded through polycarbonate membranes (0.1 μm) using an Avanti Mini-Extruder (Avanti
444 Polar Lipids, Alabaster, AL, USA).
445 The liposome pull-down assay was performed as previously described [21]. Briefly, the liposome
446 suspension was diluted five-fold in freshly prepared binding buffer (120 mM sodium citrate, pH
447 6.5) and incubated with 128 nM of either native MakA or histidine mutants, $MakA^{H30K}$ or
448 $MakA^{H95K}$. The mixtures were incubated at 37°C for 60 min and then centrifuged at 21,000 ×g for
449 30 min at room temperature. The pellets were washed two to three times with their respective
450 binding buffers to minimize background binding. Samples were resuspended in buffer, boiled, and
451 analyzed by SDS-PAGE. Proteins were then transferred to nitrocellulose membranes, blocked with
452 skim milk, and probed with anti-MakA primary antibodies (1:10,000 dilution in 5% skimmed milk)
453 overnight at 4°C. After washing, membranes were incubated with HRP-conjugated secondary
454 antibodies, and signals were visualized using a chemiluminescent substrate. Imaging was
455 performed using an ImageQuant LAS 4000 system.
456
457 **Confocal Microscopy**
458 Freshly prepared human erythrocytes (0.25%) in suspended citrate buffer (120 mM sodium citrate,
459 pH adjusted to 6.5) were prelabelled with the liphophilic dye Dil (5 μM). The labeled erythrocytes
460 were then treated with wild-type or mutant MakA proteins (1 μM) in 18-well chamber slides (μ-
461 Slide, ibidi) for 4 hours at 37°C in a 5% CO_2 incubator.
462 For binding assay with Alexa488-MakA, Alexa488-$MakA^{H30K}$, or Alexa488-$MakA^{H95K}$, freshly
463 Dil-labeled (5 μM) human erythrocytes (0.25% in citrate buffer, pH 6.5) were loaded into an eight-
464 well chamber slide (μ-Slide, ibidi) and incubated with Alexa488-MakA (1 μM) for 4 hours at 37°C
465 in a 5% CO_2 incubator.

466 For FITC-dextran uptake assays, DiI-labeled erythrocytes (0.25%) were exposed to wild-type
467 MakA or mutant ($MakA^{H30K}$ and $MakA^{H95K}$) proteins (1 μM) in citrate buffer (pH 6.5) for 4 hours
468 in 18-well chamber slides (μ-Slide, ibidi), followed by the addition of FITC-Dextran (1 mg/mL)
469 for 30 min at 37°C.
470 Liposomes prepared from SLM including or lacking cholesterol (SLM-cholesterol) were incubated
471 with Alexa568-MakA (1 μM) for 4 hours at 37°C prior to imaging. All samples were visualized
472 using a Leica SP8 inverted confocal system (Leica Microsystems) equipped with an HC PL APO
473 63×/1.40 oil immersion lens.
474
475 **Scanning Electron Microscopy**
476 Freshly prepared human erythrocytes (0.25%) were treated with MakA, $MakA^{H30K}$, or $MakA^{H95K}$
477 proteins (1 μM, 90 min) in citrate buffer (120 mM, pH 6.5). Samples were fixed with a fixative
478 solution (1% glutaraldehyde +0.1 M CaCo buffer +3 mM $MgCl_2$), followed by two washes with
479 buffer (0.1 M CaCo buffer +2.5% sucrose +3 mM $MgCl_2$). The fixed cells were allowed to sediment
480 onto poly-L-lysine-coated coverslips for 1 hour and subsequently dehydrated in a series of graded
481 ethanol solutions in the microwave. Samples were then subjected to critical point drying (Leica
482 EM300) and coated with a 2 nm platinum layer using a Quorum Q150T ES sputter coater. Imaging
483 was performed using a Carl Zeiss Merlin field-emission scanning electron microscope equipped
484 with an in-chamber (ETD) secondary electron detector at an accelerating voltage of 5 kV and a
485 probe current of 150 pA.
486
487 **Transmission Electron Microscopy (TEM)**
488 Negative staining for liposomes prepared from epithelial cell lipid extracts (ECLE) or synthetic
489 lipid mixture (SLM) was performed on glow-discharged copper grids (300 mesh) coated with a
490 thin carbon film (Ted Pella, Redding, CA) as previously described [21]. Briefly, ECLE or SLM of
491 various lipid compositions were incubated with wild-type MakA, or mutant ($MakA^{H30K}$ or
492 $MakA^{H95K}$) proteins (3 μM) for 90 min in citrate buffer (pH 6.5) before preparation for TEM. A 3
493 μL aliquot of each sample were applied to the grids, washed twice with Milli-Q water (MQ) water,
494 and stained with 1.5% uranyl acetate solution (EMS, Hatfield, PA), followed by a final wash with
495 Milli-Q water. Grids were examined using Talos L120C TEM, operated at 120 kV. Images were
496 captured with a Ceta 16M CCD camera using TEM Image & Analysis software ver. 4.17 (FEI,
497 Eindhoven, The Netherlands).
498
499 **SparkCyto image analysis**
500 The kinetics of wild-type MakA and mutant proteins, $MakA^{H30K}$ and $MakA^{H95K}$, were investigated
501 using the SparkCyto imaging system. Alexa568-MakA, Alexa568-$MakA^{H30K}$ and Alexa568-
502 $MakA^{H95K}$ (1 μM each), were incubated in the presence or absence of liposomes prepared from
503 ECLE. Images were acquired every 10 minutes for a total duration of 3.5 hours, with and without
504 ECLE liposomes. The fluorescence intensity from the images was quantified as integrated intensity
505 using Fiji ImageJ [50]. A total of four spots, each measuring 583931 μm^2, were quantified from

each image. After pooling conditions between experimental repeats, mean blank subtraction, normalization against time zero, the linear rate constants (k)/hour were calculated.

Statistical analysis

Results from replicates are presented as mean ± s.d. Statistical significance between groups was determined using one-way or two-way ANOVA, performed in GraphPad Prism. Significance levels were defined as $p < 0.05$ (*), $p < 0.01$ (**), and ns = not significant.

Acknowledgements

A.N. received support from the Swedish Research Council (2022-04779) and the Kempe Foundations (JCSMK23-0138). We acknowledge the facilities and technical assistance of the Umeå Core Facility Electron Microscopy (UCEM) and the Biochemical Imaging Center (BICU), Umeå University, a part of the National Microscopy Infrastructure NMI (VR-RFI 201600968 and VR-RFI 2019–00217). We acknowledge the Protein Expression and Purification facility (PEP) at Umeå University for construct design and cloning.

Author Contributions

All co-authors contributed to the design of experiments, data analysis, interpretation, manuscript revisions, and agree on the final contents of the manuscript.

Author Information

Correspondence and requests should be addressed to A.N.
(aftab.nadeem@umu.se)

References

[1] Geny B, Popoff MR. Bacterial protein toxins and lipids: pore formation or toxin entry into cells. Biol Cell. 2006;98:667-78.

[2] Lemichez E, Barbieri JT. General aspects and recent advances on bacterial protein toxins. Cold Spring Harb Perspect Med. 2013;3:a013573.

[3] Los FC, Randis TM, Aroian RV, Ratner AJ. Role of pore-forming toxins in bacterial infectious diseases. Microbiol Mol Biol Rev. 2013;77:173-207.

[4] Verma P, Gandhi S, Lata K, Chattopadhyay K. Pore-forming toxins in infection and immunity. Biochem Soc Trans. 2021;49:455-65.

[5] Taylor RK, Miller VL, Furlong DB, Mekalanos JJ. Use of phoA gene fusions to identify a pilus colonization factor coordinately regulated with cholera toxin. Proc Natl Acad Sci U S A. 1987;84:2833-7.

[6] Rajpara N, Vinothkumar K, Mohanty P, Singh AK, Singh R, Sinha R, et al. Synergistic effect of various virulence factors leading to high toxicity of environmental V. cholerae non-O1/ non-O139 isolates lacking ctx gene : comparative study with clinical strains. PLoS One. 2013;8:e76200.

[7] Schwartz K, Hammerl JA, Gollner C, Strauch E. Environmental and Clinical Strains of Vibrio cholerae Non-O1, Non-O139 From Germany Possess Similar Virulence Gene Profiles. Front Microbiol. 2019;10:733.

[8] Dongre M, Singh B, Aung KM, Larsson P, Miftakhova R, Persson K, et al. Flagella-mediated secretion of a novel Vibrio cholerae cytotoxin affecting both vertebrate and invertebrate hosts. Commun Biol. 2018;1:59.

[9] Nadeem A, Nagampalli R, Toh E, Alam A, Myint SL, Heidler TV, et al. A tripartite cytolytic toxin formed by Vibrio cholerae proteins with flagellum-facilitated secretion. Proc Natl Acad Sci U S A. 2021;118.

[10] Tsou AM, Zhu J. Quorum sensing negatively regulates hemolysin transcriptionally and posttranslationally in Vibrio cholerae. Infect Immun. 2010;78:461-7.

[11] Oscarsson J, Mizunoe Y, Li L, Lai XH, Wieslander A, Uhlin BE. Molecular analysis of the cytolytic protein ClyA (SheA) from Escherichia coli. Mol Microbiol. 1999;32:1226-38.

[12] Oscarsson J, Mizunoe Y, Uhlin BE, Haydon DJ. Induction of haemolytic activity in Escherichia coli by the slyA gene product. Mol Microbiol. 1996;20:191-9.

[13] Brauning B, Bertosin E, Praetorius F, Ihling C, Schatt A, Adler A, et al. Structure and mechanism of the two-component alpha-helical pore-forming toxin YaxAB. Nat Commun. 2018;9:1806.

[14] Schubert E, Vetter IR, Prumbaum D, Penczek PA, Raunser S. Membrane insertion of alpha-xenorhabdolysin in near-atomic detail. Elife. 2018;7.

[15] Sastalla I, Fattah R, Coppage N, Nandy P, Crown D, Pomerantsev AP, et al. The Bacillus cereus Hbl and Nhe tripartite enterotoxin components assemble sequentially on the surface of target cells and are not interchangeable. PLoS One. 2013;8:e76955.

[16] Wilson JS, Churchill-Angus AM, Davies SP, Sedelnikova SE, Tzokov SB, Rafferty JB, et al. (Identification and structural analysis of the tripartite alpha-pore forming toxin of Aeromonas hydrophila). Nat Commun. 2019;10:2900.

[17] Churchill-Angus AM, Schofield THB, Marlow TR, Sedelnikova SE, Wilson JS, Rafferty JB, et al. Characterisation of a tripartite alpha-pore forming toxin from Serratia marcescens. Sci Rep. 2021;11:6447.

[18] Nadeem A, Alam A, Toh E, Myint SL, Ur Rehman Z, Liu T, et al. Phosphatidic acid-mediated binding and mammalian cell internalization of the Vibrio cholerae cytotoxin MakA. PLoS Pathog. 2021;17:e1009414.
[19] Nadeem A, Aung KM, Ray T, Alam A, Persson K, Pal A, et al. Suppression of beta-catenin signaling in colon carcinoma cells by a bacterial protein. Int J Cancer. 2021;149:442-59.
[20] Toh E, Baryalai P, Nadeem A, Aung KM, Chen S, Persson K, et al. Bacterial protein MakA causes suppression of tumour cell proliferation via inhibition of PIP5K1alpha/Akt signalling. Cell Death Dis. 2022;13:1024.
[21] Nadeem A, Berg A, Pace H, Alam A, Toh E, Aden J, et al. Protein-lipid interaction at low pH induces oligomerization of the MakA cytotoxin from Vibrio cholerae. Elife. 2022;11.
[22] Junglas B, Huber ST, Heidler T, Schlosser L, Mann D, Hennig R, et al. PspA adopts an ESCRT-III-like fold and remodels bacterial membranes. Cell. 2021;184:3674-88 e18.
[23] Junglas B, Hudina E, Schonnenbeck P, Ritter I, Heddier A, Santiago-Schubel B, et al. Structural plasticity of bacterial ESCRT-III protein PspA in higher-order assemblies. Nat Struct Mol Biol. 2025;32:23-34.
[24] Chanchevalap S, Yang Z, Cui N, Qu Z, Zhu G, Liu C, et al. Involvement of histidine residues in proton sensing of ROMK1 channel. J Biol Chem. 2000;275:7811-7.
[25] Hancock RE, Sahl HG. Antimicrobial and host-defense peptides as new anti-infective therapeutic strategies. Nat Biotechnol. 2006;24:1551-7.
[26] Wang Y, Malenbaum SE, Kachel K, Zhan H, Collier RJ, London E. Identification of shallow and deep membrane-penetrating forms of diphtheria toxin T domain that are regulated by protein concentration and bilayer width. J Biol Chem. 1997;272:25091-8.
[27] Pohnl M, Trollmann MFW, Bockmann RA. Nonuniversal impact of cholesterol on membranes mobility, curvature sensing and elasticity. Nat Commun. 2023;14:8038.
[28] Jia X, Knyazeva A, Zhang Y, Castro-Gonzalez S, Nakamura S, Carlson LA, et al. V. cholerae MakA is a cholesterol-binding pore-forming toxin that induces non-canonical autophagy. J Cell Biol. 2022;221.
[29] Boyken SE, Benhaim MA, Busch F, Jia M, Bick MJ, Choi H, et al. De novo design of tunable, pH-driven conformational changes. Science. 2019;364:658-64.
[30] Kisovec M, Rezelj S, Knap P, Cajnko MM, Caserman S, Flasker A, et al. Engineering a pH responsive pore forming protein. Sci Rep. 2017;7:42231.
[31] Mihailescu M, Sorci M, Seckute J, Silin VI, Hammer J, Perrin BS, Jr., et al. Structure and Function in Antimicrobial Piscidins: Histidine Position, Directionality of Membrane Insertion, and pH-Dependent Permeabilization. J Am Chem Soc. 2019;141:9837-53.
[32] Rodnin MV, Vasques-Montes V, Kyrychenko A, Oliveira NFB, Kashipathy MM, Battaile KP, et al. Histidine Protonation and Conformational Switching in Diphtheria Toxin Translocation Domain. Toxins (Basel). 2023;15.
[33] Ilangumaran Ponmalar I, Sarangi NK, Basu JK, Ayappa KG. Pore Forming Protein Induced Biomembrane Reorganization and Dynamics: A Focused Review. Front Mol Biosci. 2021;8:737561.
[34] Shokri A, Larsson G. Characterisation of the Escherichia coli membrane structure and function during fedbatch cultivation. Microb Cell Fact. 2004;3:9.
[35] Sohlenkamp C, Geiger O. Bacterial membrane lipids: diversity in structures and pathways. FEMS Microbiol Rev. 2016;40:133-59.
[36] Beltran-Heredia E, Tsai FC, Salinas-Almaguer S, Cao FJ, Bassereau P, Monroy F. Membrane curvature induces cardiolipin sorting. Commun Biol. 2019;2:225.

[37] Huang KC, Ramamurthi KS. Macromolecules that prefer their membranes curvy. Mol Microbiol. 2010;76:822-32.
[38] Matyash V, Geier C, Henske A, Mukherjee S, Hirsh D, Thiele C, et al. Distribution and transport of cholesterol in Caenorhabditis elegans. Mol Biol Cell. 2001;12:1725-36.
[39] Merris M, Wadsworth WG, Khamrai U, Bittman R, Chitwood DJ, Lenard J. Sterol effects and sites of sterol accumulation in Caenorhabditis elegans: developmental requirement for 4alpha-methyl sterols. J Lipid Res. 2003;44:172-81.
[40] Watts JL, Ristow M. Lipid and Carbohydrate Metabolism in Caenorhabditis elegans. Genetics. 2017;207:413-46.
[41] Koyiloth M, Gummadi SN. Regulation and functions of membrane lipids: Insights from Caenorhabditis elegans. BBA Adv. 2022;2:100043.
[42] Erlandson KJ, Bisht H, Weisberg AS, Hyun SI, Hansen BT, Fischer ER, et al. Poxviruses Encode a Reticulon-Like Protein that Promotes Membrane Curvature. Cell Rep. 2016;14:2084-91.
[43] Zurek N, Sparks L, Voeltz G. Reticulon short hairpin transmembrane domains are used to shape ER tubules. Traffic. 2011;12:28-41.
[44] Bhaskara RM, Grumati P, Garcia-Pardo J, Kalayil S, Covarrubias-Pinto A, Chen W, et al. Curvature induction and membrane remodeling by FAM134B reticulon homology domain assist selective ER-phagy. Nat Commun. 2019;10:2370.
[45] Khaminets A, Heinrich T, Mari M, Grumati P, Huebner AK, Akutsu M, et al. Regulation of endoplasmic reticulum turnover by selective autophagy. Nature. 2015;522:354-8.
[46] Khattree N, Ritter LM, Goldberg AF. Membrane curvature generation by a C-terminal amphipathic helix in peripherin-2/rds, a tetraspanin required for photoreceptor sensory cilium morphogenesis. J Cell Sci. 2013;126:4659-70.
[47] Hurley JH, Hanson PI. Membrane budding and scission by the ESCRT machinery: it's all in the neck. Nat Rev Mol Cell Biol. 2010;11:556-66.
[48] Rice A, Zourou AC, Cotten ML, Pastor RW. A unified model of transient poration induced by antimicrobial peptides. Proc Natl Acad Sci U S A. 2025;122:e2510294122.
[49] Tweten RK. Cholesterol-dependent cytolysins, a family of versatile pore-forming toxins. Infect Immun. 2005;73:6199-209.
[50] Schindelin J, Arganda-Carreras I, Frise E, Kaynig V, Longair M, Pietzsch T, et al. Fiji: an open-source platform for biological-image analysis. Nat Methods. 2012;9:676-82.

651 **Figure and legends**

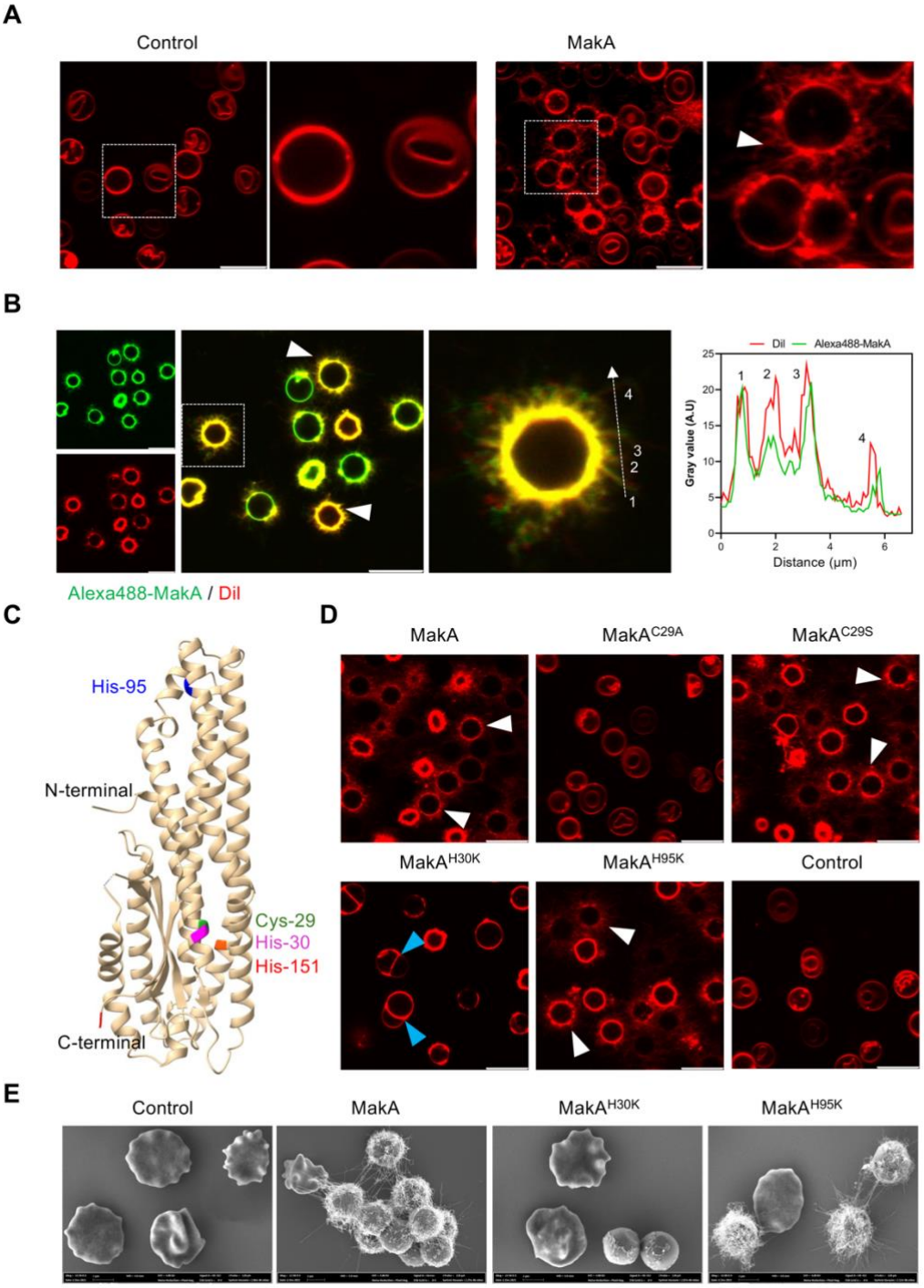

652

653 **Figure 1: The histidine residue at the N-terminus of MakA facilitates tubulation of the erythrocyte**
654 **cell membrane.**
655 **(A)** Human erythrocytes pre-labeled with the lipophilic dye DiI and suspended in citrate buffer (pH 6.5), were
656 exposed to MakA (1 μM) for 4 hours, followed by live-cell confocal microscopy. White arrowheads indicate
657 tubulation of the cell membrane. **(B)** Cell-associated MakA was visualized using Alexa488-MakA (green).
658 For co-localization experiments, DiI-labeled erythrocytes (red) were incubated with Alexa488-MakA protein

659 (1 μM) for 4 hours at pH 6.5, followed by live-cell confocal microscopy. White arrowheads indicates co-
660 localization of Alexa488-MakA with the Dil-labeled erythrocyte cell membrane. The larger panels show the
661 merged images and an enlargement of one erythrocyte as marked with a square. The line graph (right)
662 shows the fluorescence intensity profile of the corresponding merged image across the dotted white line.
663 The numbers in the image and line plot indicate co-localization of Alexa488-MakA with Dil labeled
664 erythrocyte cell membrane across four tubules. **(C)** Crystal structure of MakA monomer (PDB accession no.
665 6EZV; [8]). Point mutations introduced at the N-terminus of the protein are highlighted in blue ($MakA^{H95K}$),
666 green ($MakA^{C29A}$ or $MakA^{C29S}$), purple ($MakA^{H30K}$), and red ($MakA^{H195K}$). **(D)** Human erythrocytes labeled
667 with Dil (red) were treated with wild-type MakA or the mutant proteins (1 μM) for 4 hours at pH 6.5, followed
668 by live-cell confocal microscopy. White arrowheads indicate tubulation of the erythrocyte cell membrane in
669 response to wild-type MakA or the mutant proteins, while cyan arrowheads in $MakA^{H30K}$ treated cells indicate
670 fusion of erythrocytes. **(E)** Scanning electron microscopy (SEM) images of erythrocytes treated with wild-
671 type or mutant proteins (1 μM, 90 min) in citrate buffer (pH 6.5) are shown. Representative micrographs of
672 erythrocytes indicate the formation of tubular structures on their cell membrane upon exposure to the wild-
673 type MakA or its mutant protein, $MakA^{H95K}$. Membrane perturbation, but lack of tubulation, was observed in
674 the erythrocytes exposed to the mutant protein, $MakA^{H30K}$.

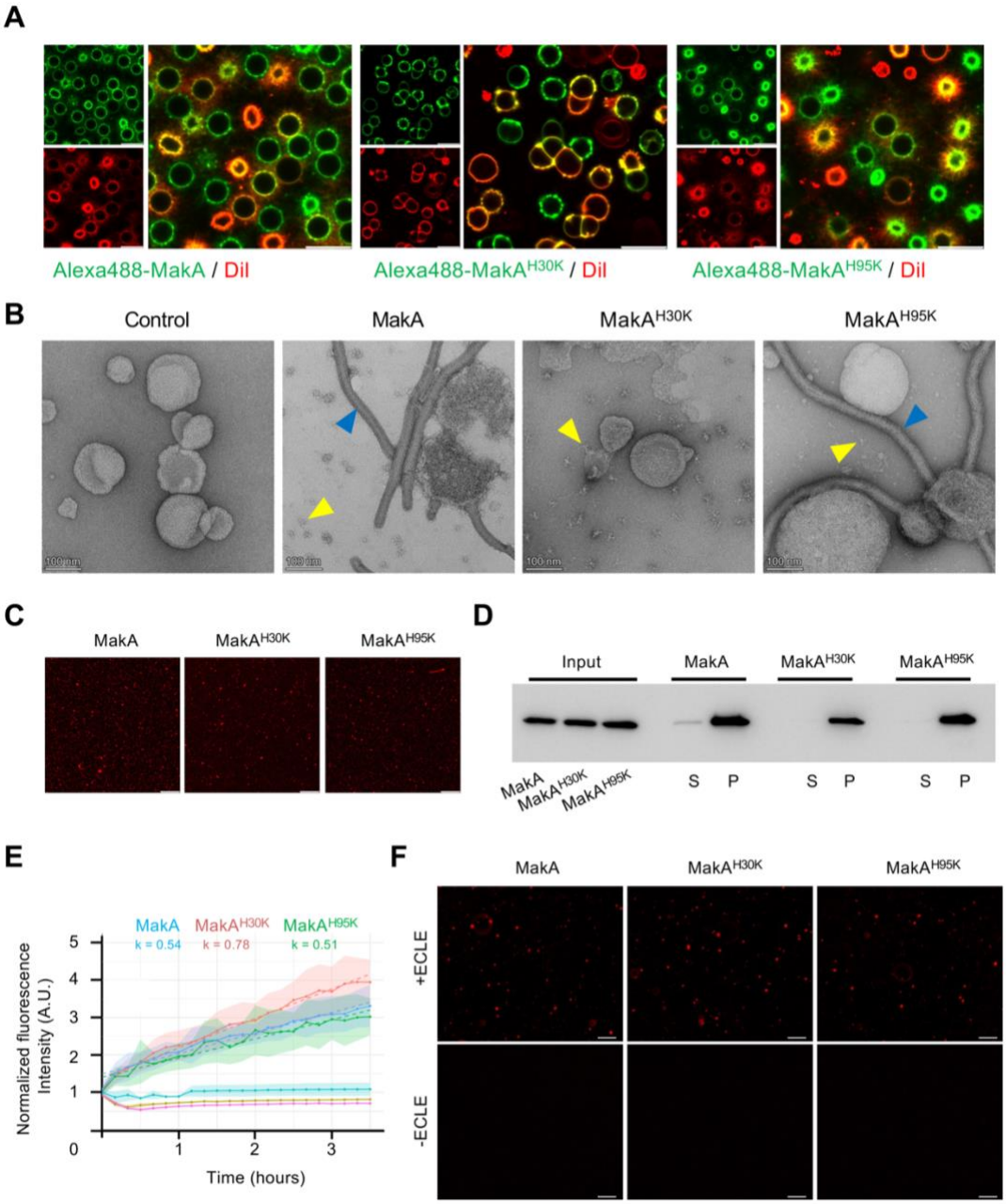

Figure 2: The N-terminus histidine mutant of MakA binds to the lipid membrane but lacks tubulation. (A) Cell-associated Alexa488-labeled wild-type MakA or the mutant proteins MakA^{H30K} and MakA^{H95K} were visualized using confocal microscopy. For co-localization experiments, DiI-labeled erythrocytes (red) were incubated with the wild-type Alexa488-MakA, and the mutant proteins, Alexa488-MakA^{H30K} or Alexa488-MakA^{H95K} (1 μM at pH 6.5) for 4 hours, followed by live-cell confocal microscopy. The larger panels show merged images. Scale bars = 10 μm. **(B)** Liposomes prepared from epithelial cell lipid extract (ECLE) were treated with the wild-type MakA or the mutant proteins (1 μM at pH 6.5) for 90 min and negatively stained with a 1.5% uranyl acetate solution. Images were captured with transmission electron microscopy (TEM). Blue arrowheads indicate tubular structures, while yellow arrowheads indicate the formation of MakA oligomeric structures present adjacent to or associated with liposomes. Scale bars, 100 nm. **(C)** ECLE liposomes were exposed to wild type Alexa488-MakA or the mutant proteins, Alexa488-MakA^{H30K} or Alexa488-MakA^{H95K} (1 μM at pH 6.5) for 90 min, followed by confocal microscopy. Scale bars = 5 μm. **(D)** Western blot analysis of liposome-bound wild-type MakA and the mutant proteins, MakA^{H30K} or MakA^{H95K}

689 were detected with the anti-MakA antisera. MakA proteins (128 nM) were incubated in citrate buffer (120
690 mM, pH 6.5) with liposomes prepared from epithelial cell lipid extracts. The pellet indicates liposome bound,
691 while supernatant indicates unbound wild-type MakA or the mutant proteins, $MakA^{H30K}$ and $MakA^{H95K}$. S =
692 supernatant; P = pellet. Equal concentrations of MakA and its mutant proteins were used as an input. **(E)**
693 SparkCyto image analysis for the kinetics of the wild-type MakA, and its histidine mutants ($MakA^{H30K}$ and
694 $MakA^{H95K}$, respectively) binding to liposomes prepared from ECLE. Images were acquired each 10 min for
695 a duration of 3.5 hours. k = linear rate constant per hour. **(F)** Representative SparkCyto images of ECLE
696 liposomes exposed to Alexa488 labeled wild-type MakA, or the mutant ($MakA^{H30K}$ and $MakA^{H95K}$) proteins
697 (1 μM) for 3.5 hours. Scale bars = 20 μm.
698

699

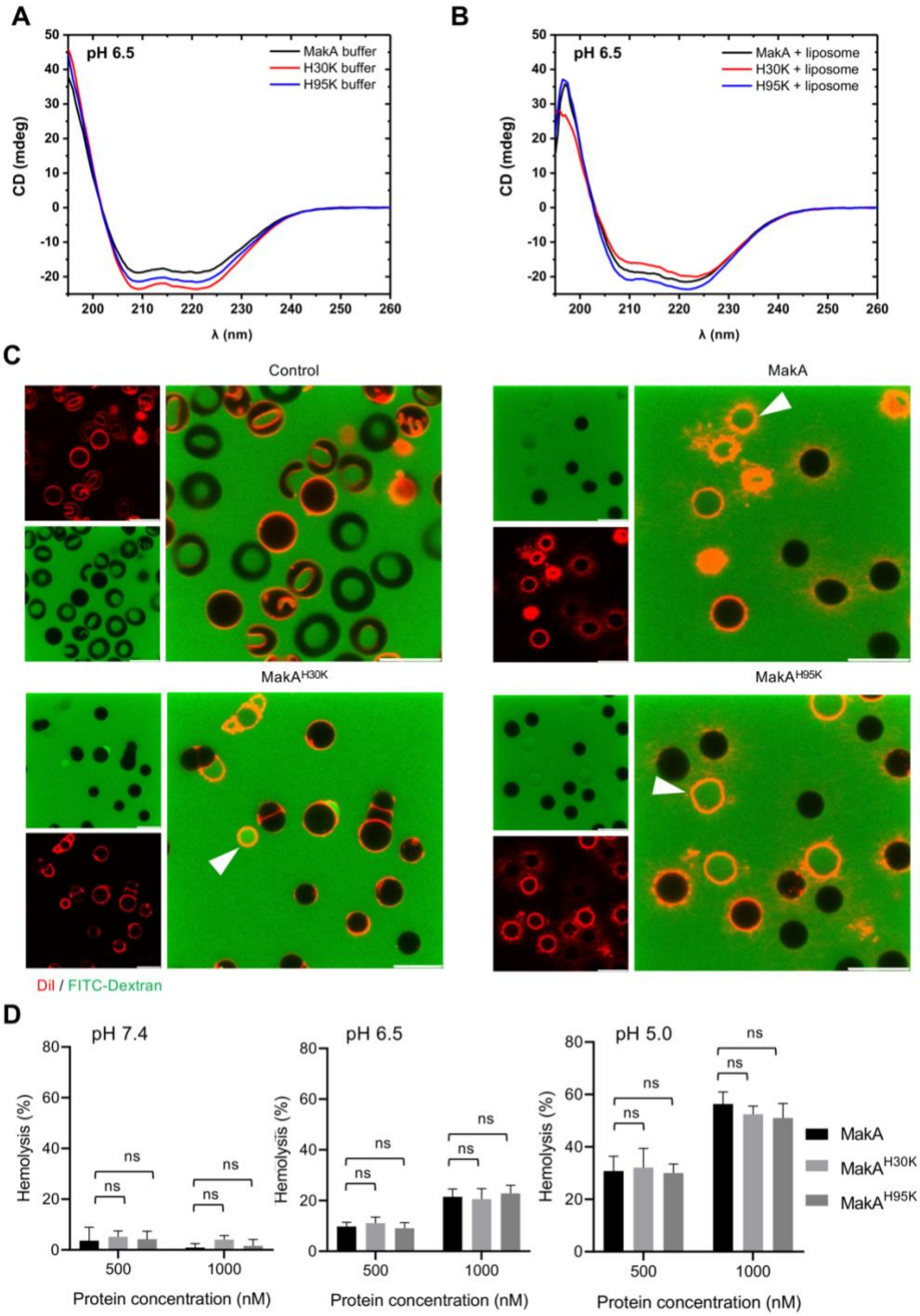

700
701 **Figure 3: MakA-induced lysis of human erythrocytes does not depend on the pH-sensing His30**
702 **residue.**
703 Far-UV circular dichroism (CD) spectra of wild-type MakA and the mutant ($MakA^{H30K}$ or $MakA^{H95K}$) proteins
704 were recorded in the absence **(A)** or presence **(B)** of liposomes prepared from ECLE. CD spectra were
705 obtained in citrate buffer (5 mM, pH 6.5) using 3 µM protein. The absorption intensity measured from buffer-
706 only controls was subtracted to correct background absorption. **(C)** Human erythrocytes pre-labeled with DiI
707 were suspended in citrate buffer (pH 6.5) and exposed to wild-type MakA or the mutant ($MakA^{H30K}$ or

708 MakA^{H95K}) proteins (1 μM at pH 6.5) for 4 hours, followed by live-cell confocal microscopy. FITC-Dextran
709 (green, 1 mg/mL) was added to the extracellular medium to assess cell permeability. White arrowheads
710 indicate erythrocyte lysis. **(D)** Human erythrocytes suspended in citrate buffer (pH 6.5) were treated with
711 increasing concentration of wild-type MakA or its mutant (MakA^{H30K} or MakA^{H95K}) proteins for 5 hours.
712 Hemolytic activity was quantified by measuring released hemoglobin and normalized to erythrocytes treated
713 with 0.1% Triton X-100 (set as 100% lysis). Data are representative of two independent experiments; bar
714 graphs show means ± s.d. Significance from the replicates was determined using two-way ANOVA with
715 Tukey's multiple comparison test. ns = not significant.
716

717

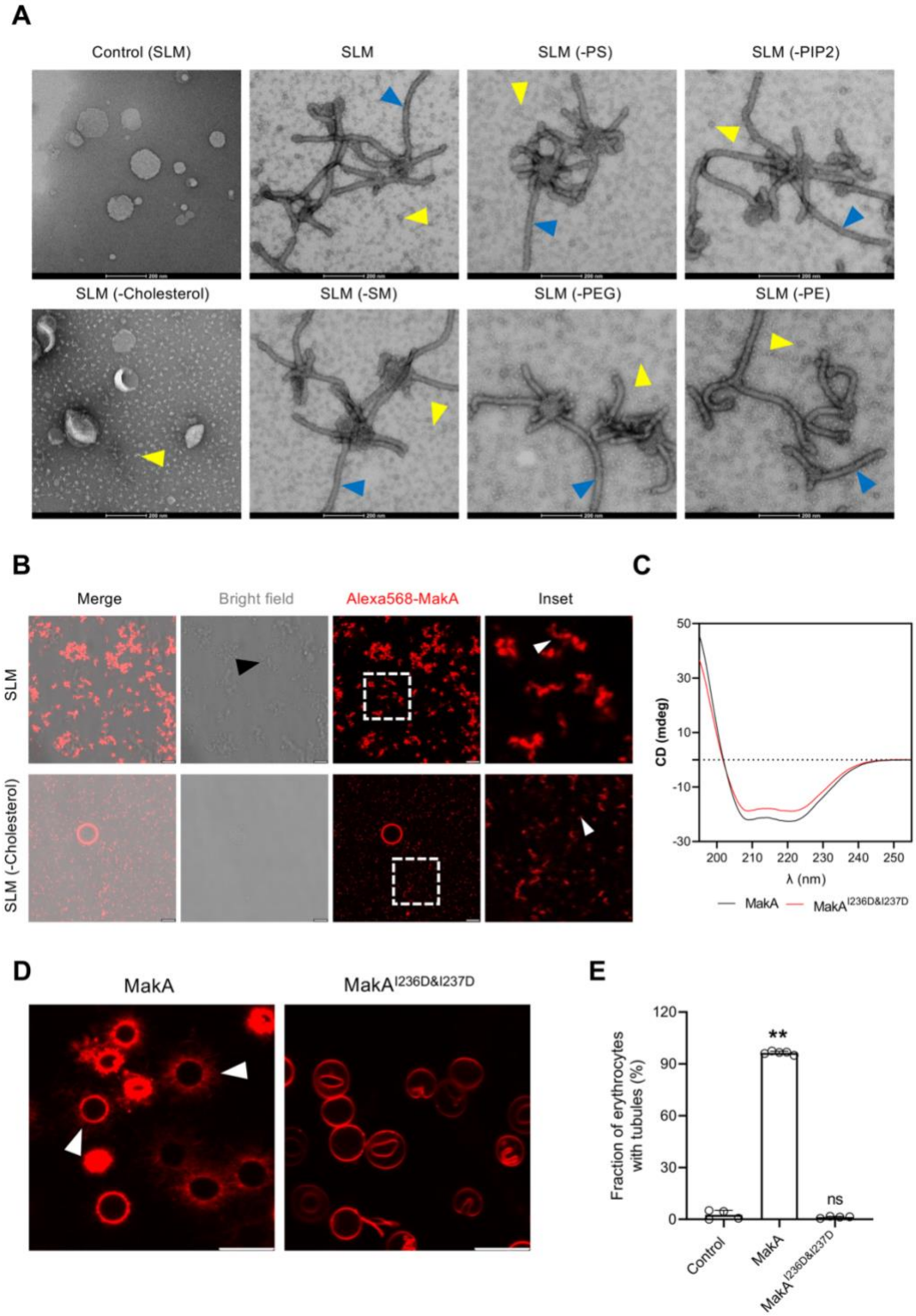

718

719 **Figure 4: Cholesterol contributes to induction of lipid membrane tubulation in response to MakA**
720 **(A)** TEM images of synthetic lipid mixture (SLM) liposomes after incubation with MakA (3 μM, 90 min) in
721 citrate buffer (pH 6.5). Robust tubulation was observed in all SLM variants except those lacking cholesterol.
722 Blue arrowheads indicate tubular structures, while yellow arrowheads indicate the formation of MakA
723 oligomeric structures present nearby or on liposomes. Scale bars, 200 nm. **(B)** Confocal microscopy of

724 Alexa568-labeled MakA (3 μM , 4 hours at pH 6.5) incubated with SLM liposomes containing or lacking
725 cholesterol. Reduced fluorescence and liposome aggregation (shown with black arrowhead) were observed
726 in the absence of cholesterol, indicating impaired MakA binding. White arrowheads indicate liposome-bound
727 MakA. Scale bars, 5 μm. **(C)** Far-UV circular dichroism (CD) spectra of wild-type MakA and the mutant
728 ($MakA^{I236D\&I237D}$) protein were recorded in phosphate buffer (pH 6.5) using 3 μM protein. The absorption
729 intensity measured from buffer-only controls was subtracted to correct for background. **(D)** Confocal
730 microscopy analyses of human erythrocytes labeled with the lipophilic dye Dil (red) exposed to wild-type
731 MakA or the mutant ($MakA^{I236D\&I237D}$) protein (1 μM) in citrate buffer (pH 6.5) for 4 hours. White arrowheads
732 indicate membrane tubulation of erythrocytes. **(E)** The histogram indicates quantification of number of
733 erythrocytes with tubules (n = 156 to 214 cells / field of view) as shown in panel D. The data point represents
734 quantification of number of erythrocytes from 4 to 5 fields of view (180 x 180 μm^2), collected from two
735 independent experiments. Data is presented as mean ± s.e.m.; one-way analysis of variance (ANOVA) with
736 Sidak's multiple comparisons test. $^{**}p \leq 0.01$, ns = not significant.
737

Supplementary Information

Mechanisms involved in the lipid membrane tubulation activity of the pH-responsive MakA protein from *Vibrio cholerae*

Athar Alam[1], Abdelbasset Yabrag[2,3], Naeem Ullah[2,3], Rasmus Sten[2,3], Jörgen Åden[2], Nandita Bodra[3,4], Hudson Pace[1,3,5], Marta Bally[1,3,5], Karina Persson[3,4], Bernt Eric Uhlin[2,3], Sun Nyunt Wai[2,3,6], Aftab Nadeem[2,3]

[1]Department of Clinical Microbiology, Umeå University, Umeå, Sweden

[2]Department of Molecular Biology, Umeå University, Umeå, Sweden

[3]Umeå Centre for Microbial Research (UCMR), Umeå University, Umeå, Sweden

[4]Department of Chemistry, Umeå University, Umeå, Sweden.

[5]Wallenberg Centre for Molecular Medicine, Umeå University, Umeå, Sweden

[6]The Laboratory for Molecular Infection Medicine Sweden (MIMS), Umeå University, Umeå, Sweden

Corresponding author: aftab.nadeem@umu.se

757

758

759

760

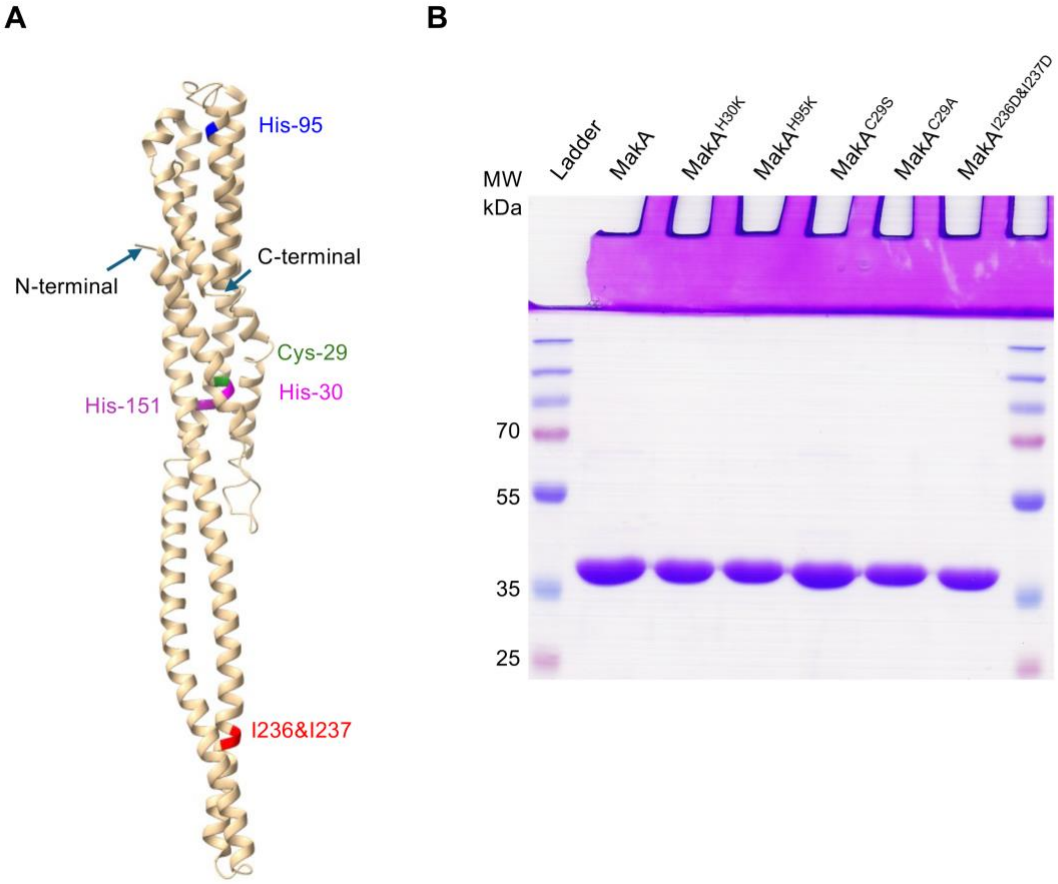

761

762

763 **Supplementary Figure 1: Wild-type and mutant MakA proteins used in this study.**
764 **(A)** Cryo-EM structural model of a subunit in the polymeric MakA tube (PDB accession no. 7P3R; [21]),
765 highlighting the residues of MakA subject to site-directed mutagenesis and used in the current study. **(B)**
766 SDS-PAGE and Coomassie Blue staining analysis of the recombinantly produced wild-type MakA and
767 substitution mutant proteins used in this study.
768

769

770

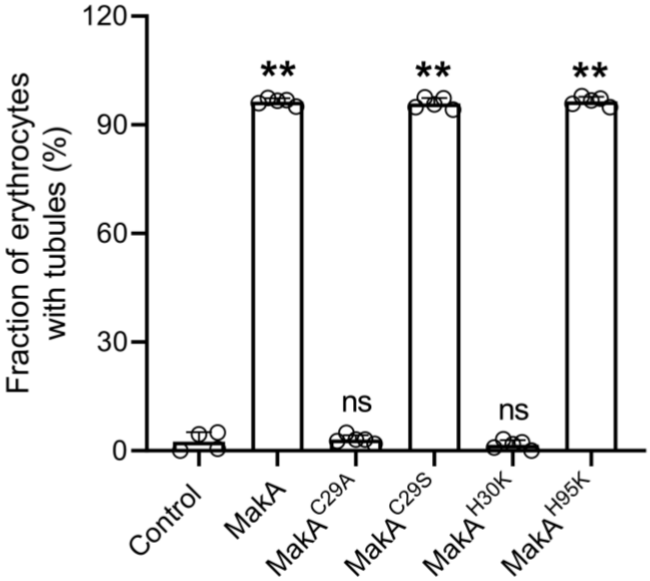

771

772 **Supplementary Figure 2: Tubulation of erythrocytes in response to MakA mutants**
773 Human erythrocytes labeled with the lipophilic dye DiI (red) were treated with wild-type
774 MakA or its mutants (1 μM) proteins for 4 hours at pH 6.5, followed by live-cell confocal
775 microscopy. The histogram indicates quantification of number of erythrocytes with tubules
776 (n = 156 to 214 cells / field of view) as shown in (Figure 1D). The data point represents
777 quantification of number of cells from 4 to 5 fields of view (180 x 180 μm^2), collected from
778 two independent experiments. Data is presented as mean ± s.e.m.; one-way analysis of
779 variance (ANOVA) with Sidak's multiple comparisons test. **$p \leq 0.01$, ns = not significant.

780 **Table S1:** Secondary structure contents (%) of wild-type MakA and histidine substitution
781 mutant proteins, as analyzed by CD spectroscopy (190–260 nm) at pH 6.5, in the
782 presence or absence of liposomes.

783

	MakA	MakA^{H30K}	MakA^{H95K}	MakA +ECLE liposomes	MakA^{H30K} +ECLE liposomes	MakA^{H95K} +ECLE liposomes
Helix	64.7	33.3	42.1	34.9	21.7	27.4
Antiparallel	0.6	8.7	4.9	8.6	18.5	12.7
Parallel	6.0	6.3	6.3	6.0	5.8	6.2
Beta-turn	11.1	16.7	15.4	17.0	18.4	17.4
Random coil	16.0	25.8	21.9	23.2	32.5	30.1
Total Sum	98.4	90.8	90.6	89.7	96.9	93.8

784

785 ## References

786 [21] Nadeem A, Berg A, Pace H, Alam A, Toh E, Aden J, et al. Protein-lipid interaction at low pH
787 induces oligomerization of the MakA cytotoxin from Vibrio cholerae. Elife. 2022;11.

788